Electronic Supplementary Information

Efficient Numerical Modelling of Magnetophoresis in Millifluidic Systems

Johannes Soika,[a]* *Tobias Wanninger*,[a] *Patrick Muschak*,[b] *Anja Schnell*,[a] *Sebastian P. Schwaminger*,[b,c,d] *Sonja Berensmeier*,[b,e] *and Markus Zimmermann* [a]

[a]: Laboratory for Product Development and Lightweight Design, Tum School of Engineering and Design, Technical University of Munich, Boltzmannstr. 15, 85748 Garching, GER.

[b]: Chair of Bioseparation Engineering, Tum School of Engineering and Design, Technical University of Munich, Boltzmannstr. 15, 85748 Garching, GER.

[c]: Division of Medicinal Chemistry, Otto Loewi Research Center, Medical University of Graz, Neue Stiftingtalstraße 6, 8010 Graz, AT.

[d]: BioTechMed-Graz, Mozartgasse 12, 8010 Graz, AT.

[e]: Munich Institute for Integrated Materials, Energy and Process Engineering, Technical University of Munich, Lichtenbergstr. 4a, 85748 Garching, GER.

*To whom correspondence should be addressed: johannes.soika@tum.de

Supplementary Information S1: Simple Models

The velocity profile of the simple model is plotted in Figure S 1. The values of Table 2 and equation 9 [1] of the main article are used. The highest velocity (dark red) appears in the middle of the channel's cross-section, while at the channel walls, the velocity is zero due to the no-slip condition. The peak velocity is $0.0169\frac{m}{s}$.

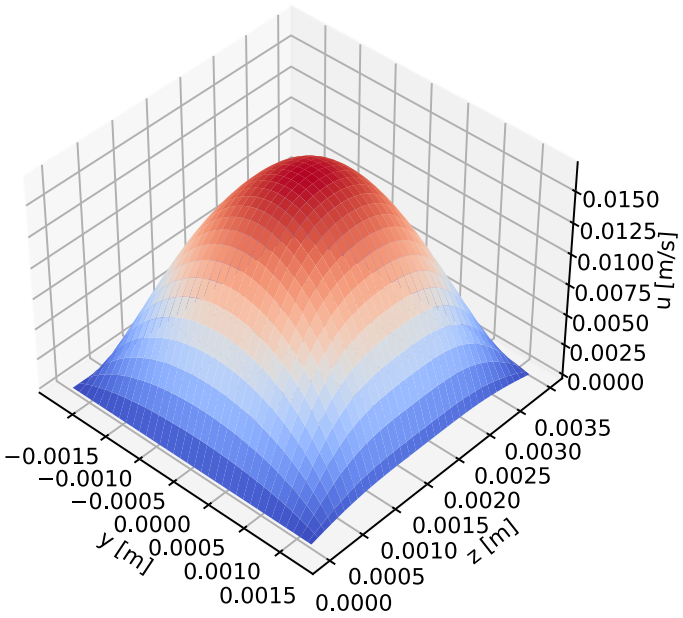

Figure S 1: Fluid velocity in rectangular channel as per equation 9.

Figure S 2 demonstrates the algorithm that identifies the separation height for a constant initial y-position, varying the z-position. The channel's upper and lower walls are represented by the black and yellow lines, respectively. The background colour indicates the field strength, with red denoting the highest strength (particularly at the magnet position, notably at the poles) and dark blue representing a minute fraction of the strength (less than 1% of the maximum). Red trajectories signify an escape from the channel, while blue trajectories reach the ground, resulting in separation. The first trajectory begins at the top of the channel, descending in equidistant steps until the first particle is separated. Subsequently, a step decay occurs, leading to progressively smaller steps and convergence to the maximum initial height from where the particles get attracted: the separation height.

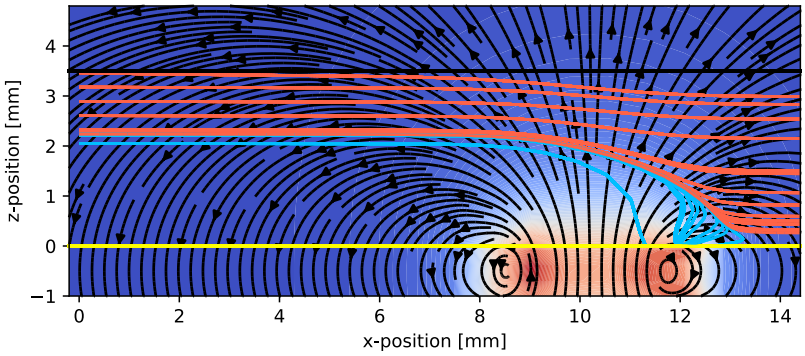

Figure S 2: Trajectories in 2D for fixed y-position. In the background, the magnetic field lines are visualised, together with a color map of the strength of the magnetic field. Red indicates a high field strength, blue a low field strength.

Number of evaluation planes

A convergence analysis was performed to determine the necessary number of evaluation planes for the 3D model. Figure S 3 shows that beyond five planes, additional planes do not improve accuracy but do increase computational costs. To ensure reliability, six planes are recommended and were used for the parameter studies presented in this research.

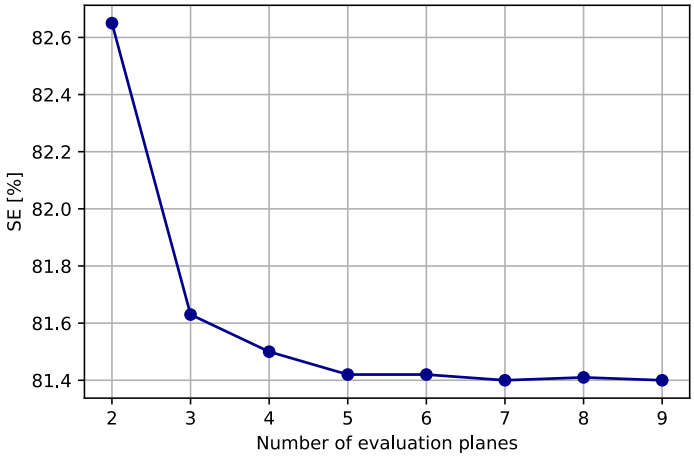

Figure S 3: Convergence analysis on the number of required evaluation planes

Supplementary Information S2: Model Comparison

In literature, the separation efficiency is often defined as the ratio between separation height to channel height $SE = \frac{h_{sep}}{h_{ch}}$ [2], [3], [4]. As shown in the paper, this might not represent the real case and might not match the evaluation procedure for experimental investigations. As shown for the 2D case in section 3.4 of the main article, considering the particle flux, a post-processing step is required to calculate the SE. In Figure S 4, the post-processing step converts

the grey line to the blue line, as per equation 3.2 of the main article. As shown in Figure 6 of the main article, this leads to a difference of up to 10% due to the post-processing step. For the 3D case, the separation line is not constant but a bathtub-shaped curve, whose shape depends on several influences. Therefore, the deviation cannot be generalised for the 3D case as in the 2D case.

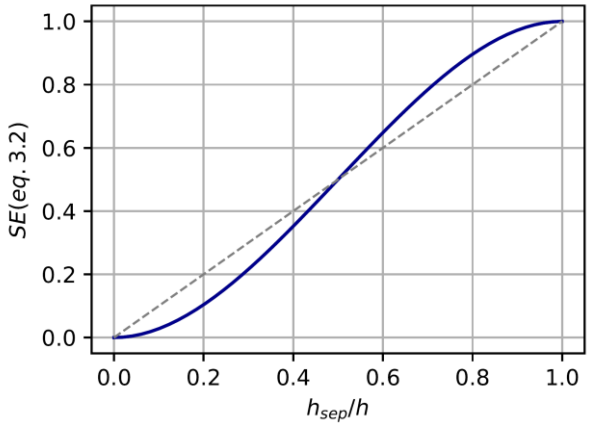

Figure S 4: Deviation calculation of SE for the 2D parabolic model.

Supplementary Information S3: FEM Modell Details

This section gives more information about the FEM model implemented in COMSOL Multiphysics 6.2.

Figure S 5 demonstrates the geometry used in the FE model. An air sphere is placed around the system to simulate the magnetic field. The sphere must be large enough to avoid deviations in the simulations. Investigations have shown that it needs to be at least twice the size of the channel.

The coordinate system is placed 5mm away from the channel's entrance. This is due to inlet effects, that can be seen in Figure S 7 and Figure S 8. Velocity deviations can be seen in the

proximity of the inlet that lead to a deflection of the particle trajectories. Therefore, the inlet positions are taken 5mm later so ensure similar conditions to the simple models.

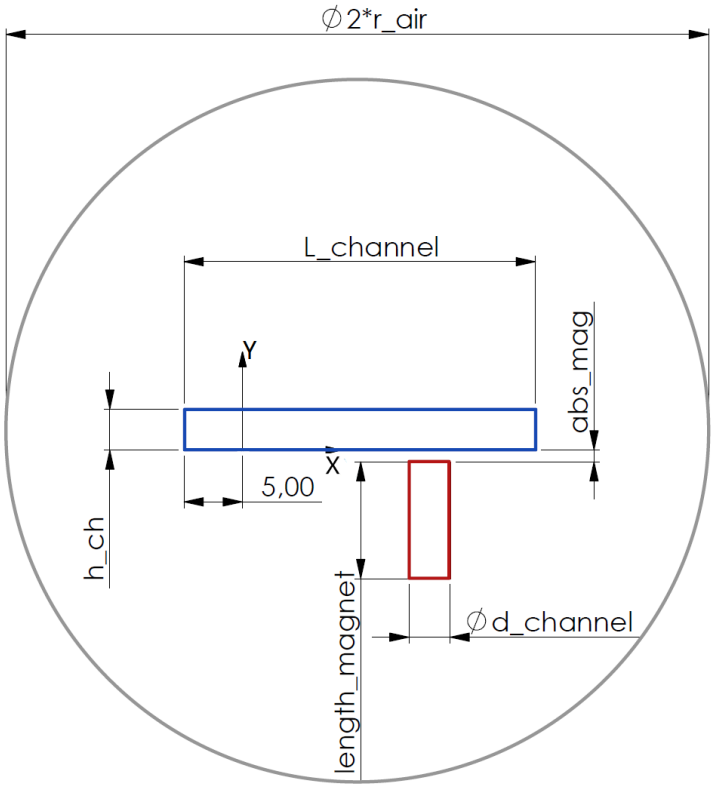

Figure S 5: Relevant geometrical parameters in the COMSOL model. The blue part represents the channel, while the magnet is shown in red. Note: The y-axis is confused with the z-axis!

A convergence analysis has been performed for the different elements. Especially the resolution of the mesh within the channel has a significant influence on the result. The convergence analysis is performed by simulating several trajectories of MNP within the

channel, subjected to a small magnetic field, so that the particles get deflected, but not separated. The average outlet z-position is taken as a reference.

The common physics-controlled mesh settings in COMSOL 6.2 have been used. Convergence analysis in Figure S 6 shows that the setting “finer” with 28374 elements for a channel of the size 35mm x 3.5mm x 3.5mm is a good trade off between accuracy and simulation time.

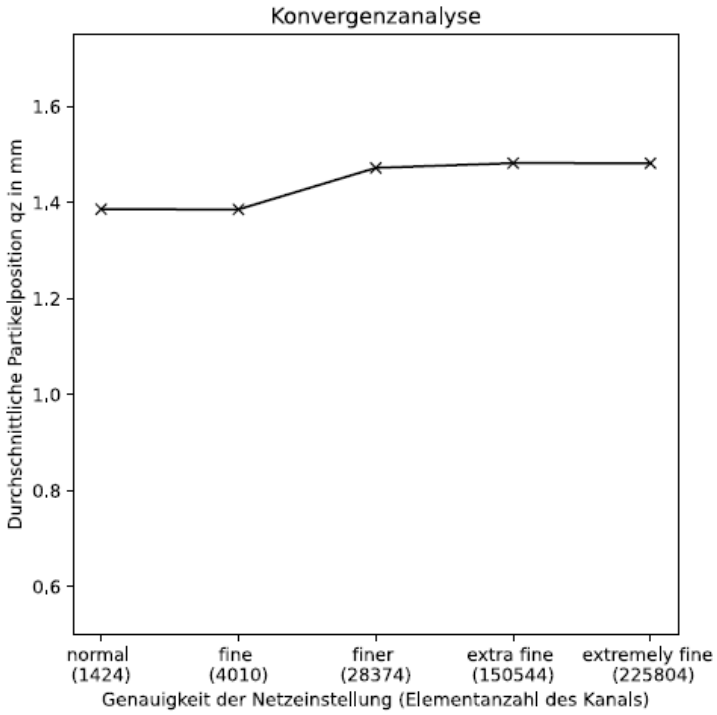

Figure S 6: Convergence analysis of the COMSOL model. On the horizontal-axis is the mesh settings and its number of elements. On the vertical-axis there is the averaged particle position at the outlet.

Even with the inlet setting “developed flow”, the velocity is perturbated at the inlet and outlet of the channel, as Figure S 7 reveals. However, from the position “0” on the flow velocity

appears to be independent of the x-position along the channel. Therefore, the model creates a similar velocity field as the field of the simple model in Figure S 1.

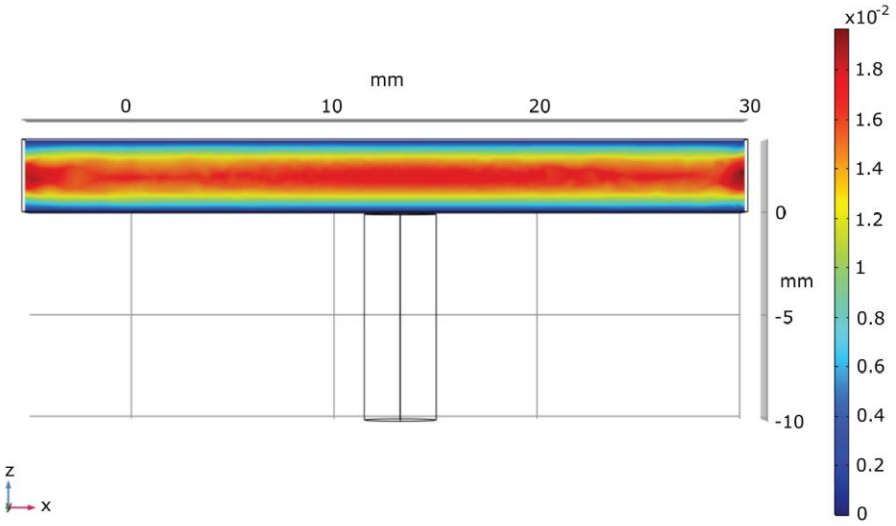

Figure S 7: Velocity profile within the channel with the inlet setting "developed flow" and the mesh "finer". The color scale bar represents the velocity in [m/s].

The trajectories of the FEM model are shown in Figure S 8. The particles start from an equally spaced grid. The deflection of the trajectories at the inlet can be seen. Near the magnet, the particles are deflected due to magnetic forces.

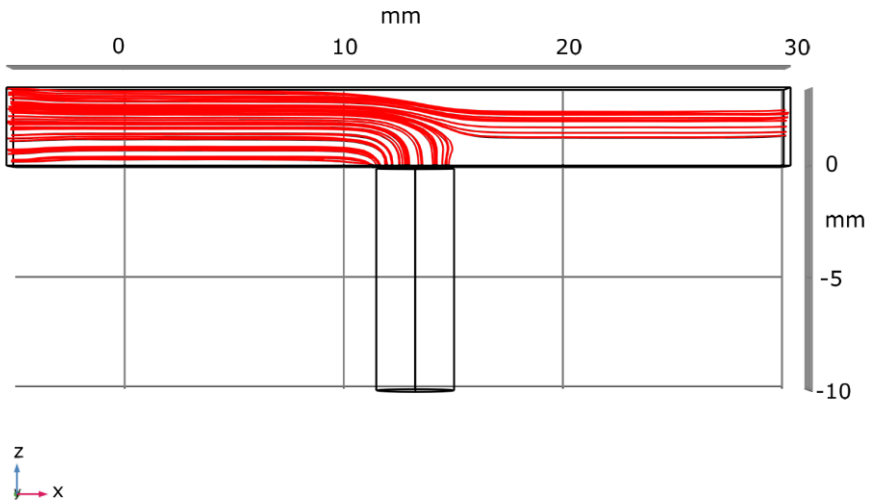

Figure S 8: Trajectories of the FEM model for the settings of table 2 of the main article.

Calculation of the separation height and simulation time

The Calculation of one trajectory in the FEM model takes in average 90 seconds on a workstation with an AMD Ryzen 7 6800H. The duration highly depends on the flow velocity and thus on the initial particle position and volume flux. The separation height is determined

differently by the FEM model. First, four initial particle positions are set along the channel height. From that, the information is extracted between which height the particles get separated. Then, two positions in between these heights are used to further narrow the interval where the particle gets separated. After four iterations, the interval is as big as $\frac{1}{4^4} = 0.39\%$ of the channel height, which is small enough to avoid calculation errors. Therefore, to obtain one separation height $4 + 2 + 2 + 2 = 10$ trajectories are necessary. To get one separation curve, six different separation heights are used. Therefore, 60 trajectories are needed, leading to a total simulation time of $60 \cdot 90\text{s} = 5400\text{s}$ which represents 1.5 hours of total simulation time. Compared to the simple 3D rectangular model, which needs 20-30 seconds, the simple 3D rectangular model is $\frac{5400\text{s}}{30\text{s}} = 180$ times fast than the FEM model.

Supplementary Information S4: Comparison FEM & Simple Models

To ensure comparability between the models, the physical fields can be compared. As shown in table 4 in the main article, the peak velocity of the simple 3D model and the FEM model deviates $0.1e-3\,\frac{\text{m}}{\text{s}}$ which is less than 2% of the maximum velocity.

Figure S 9 compares the magnetic field gradients in z-direction of the two models. As per equation 5 in the main article, the gradient, and especially the gradient in z-direction, is relevant for the magnetic force on the particle. The comparison of both fields shows a good agreement between the models, and therefore almost no deviation in magnetic field gradient.

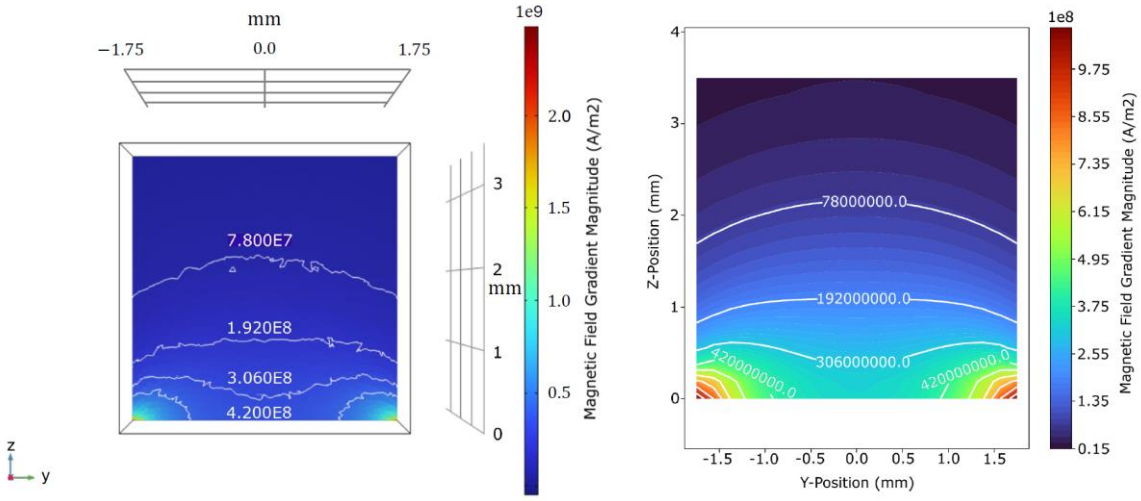

Figure S 9: Comparison of the magnetic field gradient in z-direction above the magnet. The left plot is recorded in COMSOL, while the right plot is the result of the simple model.

Comparing the SE of the FEM model to the simple 3D model shows good agreement across different settings for magnet, channel, flow conditions and MNP volumes. Table S 1 shows the results of the simulation models for different design variables settings, specified in the first column. Generally, the deviations are less than 2%.

Table S 1: Deviations between the simple 3D rectangular model and the FEM model for various design variable settings. The first column shows the design variable that got changed compared to the settings from Table 2 of the main article.

	SE 3D rectangular	**SE 3D FE**	**Difference 3D rectang. – 3D FE**
Variation channel height [m]			
h=0.0035*0.5	99,8998%	99,8988%	0,0010%
h=0.0035*1.0	81,3100%	79,3449%	1,9651%
h=0.0035*1.5	56,4602%	54,5185%	1,9417%
h=0.0035*2.0	43,0810%	41,7302%	1,3508%
Variation volume flux [m^3/s]			
$\dot{V} = 0.5e-7$	99,0823%	98,0475%	1,0348%
$\dot{V} = 0e-7$	81,3100%	79,3449%	1,9651%
$\dot{V} = 1.5e-7$	70,8436%	69,3348%	1,5088%
$\dot{V} = 2.0e-7$	63,6406%	62,1429%	1,4977%
Variation Magnetic Particle Volume [m^3]			
V_mnp=1.0e-18	54,8669%	53,6770%	1,1899%
V_mnp=4.93e-18	81,3100%	79,3449%	1,9651%
V_mnp=7.5e-18	88,8712%	87,4838%	1,3874%
Variation Polarization [mT]			
magnetization=1000	61,0517%	59,4419%	1,6098%
magnetization=1300	74,0130%	72,5682%	1,4448%
magnetizatuin=1500	81,3100%	79,3449%	1,9651%

Supplementary Information S5: Magnetic Nanoparticle Characteristics

The bare iron oxide nanoparticles utilized for this analysis were synthesized with the classical co-precipitation process via the Massart process [5, 6].

Two solutions were prepared using degassed, deionized water. First, $28.8\ g$ of $NaOH$ (Carl Roth, CAS-No.: 144-55-8) was dissolved in $400\ ml$ water, while 34.6 g of $FeCl_3(H_2O)_6$ (Carl Roth, CAS-No.: 10025-77-1) and $14.0\ g$ of $FeCl_2(H_2O)_4$ (Merck KGaA, CAS-No.: 13478-10-9) were

dispersed in $160\ ml$ of water. The reaction was carried out in a $1\ l$ round-bottom flask under a nitrogen atmosphere, placed in a water bath at $25\ °C$ on a magnetic stirrer to maintain temperature control. The $NaOH$ solution was added first, followed by the gradual addition of the iron solution, which immediately caused the precipitation of Fe_3O_4 particles. The mixture was stirred for 30 minutes at $25\ °C$. Afterwards, the solution was transferred to a $1\ l$ glass flask and washed with degassed, deionized water. The particles were separated by magnetic decantation, removing the supernatant and replacing it with fresh degassed and deionized water until the conductivity of the suspension dropped below $150\ \mu S/cm$. The synthesized particles were then stored at $4\ °C$ in a nitrogen atmosphere, with the flask sealed using parafilm.

The hydrodynamic diameter of the agglomerated nanoparticles was determined using dynamic light scattering (DLS). Therefore, $1\ ml$ dilution with a concentration of $1\ g/l$ at pH 7 was prepared in deionized water, and $900\ \mu l$ was transferred to a cuvette type DTS0012 (Malvern Instruments). Triplicate measurements were performed with a Zetasizer Ultra (Malvern Instruments) at 25 °C with an equilibration time of $120\ s$, scanning for sizes between 0.3 and $1E+4\ nm$. The particle distribution by number is depicted in Figure S 10.

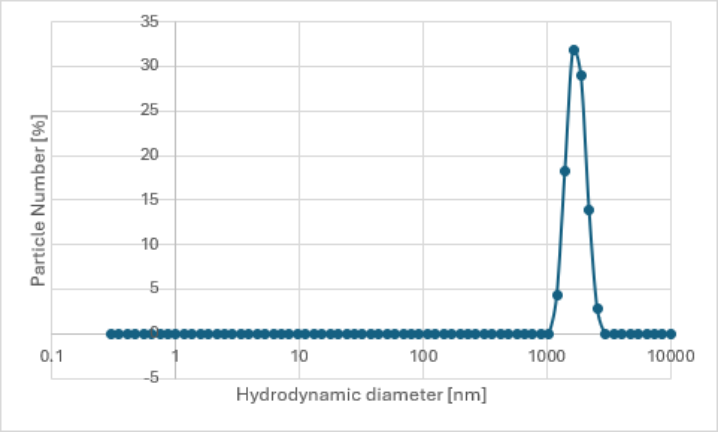

Figure S 10: Distribution of hydrodynamic diameter measured with dynamic ligth scattering.

Supplementary Information S6: Influence of the Aspect Ratio on the Model Deviation

The deviation between the models is widely discussed in the paper. However, the impact of individual variables on these deviations remains unclear. This section evaluates the influence of the aspect ratio $\frac{h}{b}$ on the deviations between the models. Since the deviation is largely dependent on the SE value itself, this influence is controlled by adjusting the aspect ratio while

modifying other design variables to maintain the same SE. Achieving an exact SE is challenging and would require an iterative process; therefore, a bandwidth of 5% was chosen to provide more data points for comparison. Figure S 11 shows the results depending on the aspect ratio of the channel for a bandwidth of $63\% < SE < 68\%$. An increase in channel height to width ratio leads to smaller deviations between the 3D simple model and the 2D models. This effect is consistent for other SE values as well.

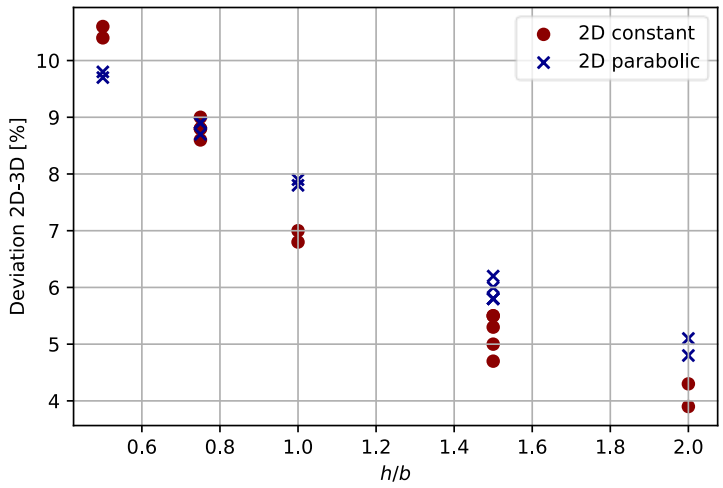

Figure S 11: Deviations between the 2D models and the simple 3D model plotted over the aspect ratio h/b of the channel. The SE of the points lies between 63% and 68%.

References

[1] H. Bruus, *Theoretical Microfluidics*. Oxford University Press, 1997. doi: 10.1093/oso/9780199235087.001.0001.

[2] P. H. Chong *et al.*, 'Continuous Flow Low Gradient Magnetophoresis of Magnetic Nanoparticles: Separation Kinetic Modelling and Simulation', *J Supercond Nov Magn*, vol. 34, no. 8, pp. 2151–2165, 2021, doi: 10.1007/s10948-021-05893-z.

[3] K. Nandy, S. Chaudhuri, R. Ganguly, and I. K. Puri, 'Analytical model for the magnetophoretic capture of magnetic microspheres in microfluidic devices', *Journal of Magnetism and Magnetic Materials*, 2008.

[4] Y. W. Tan, S. S. Leong, J. Lim, W. M. Yeoh, and P. Y. Toh, 'Low-gradient magnetic separation of magnetic nanoparticles under continuous flow: Experimental study, transport mechanism and mathematical modelling', *ELECTROPHORESIS*, vol. 43, no. 21–22, pp. 2234–2249, 2022, doi: 10.1002/elps.202200078.

[5] R. Massart, *'Preparation of aqueous magnetic liquids in alkaline and acidic media',* IEEE Transactions on Magnetics, vol. 17, issue 2, March 1981, doi: 10.1109/TMAG.1981.1061188

[6] S. Laurent et al., '*Magnetic Iron Oxide Nanoparticles: Synthesis, Stabilization, Vectorization, Physicochemical Characterizations, and Biological Applications',* American Chemical Society, vol. 108, issue 6, June 2008, doi: https://doi.org/10.1021/cr068445e

[7] M. Rodriguez et al., *'On the Distribution of Magnetic Moments in a System of Magnetic Nanoparticles'*, Multidisciplinary Digital Publishing Institute, vol. 8, issue 10, October 2022, doi: https://doi.org/10.3390/magnetochemistry8100129

[8] R. Eisenberg, H. Gray, *'Preface on Making Oxygen'*, American Chemical Society, vol. 47, issue 6, March 2008, doi: https://doi.org/10.1021/ic800155g

[9] F. Schweser et al., *'Differentiation between diamagnetic and paramagnetic cerebral lesions based on magnetic susceptibility mapping',* Wiley, vol. 37, issue 10, September 2010, doi: https://doi.org/10.1118/1.3481505

[10] N. Walker, ' Paramagnetic properties of Fe(II) and Fe(III)', American Chemical Society, vol. 54, issue 7, July 1977, https://doi: 10.1021/ed054p431.1